Proceedings of the IASS 2024 Symposium
Redefining the Art of Structural Design
August 26-30, 2024, Zurich Switzerland
Philippe Block, Giulia Boller, Catherine DeWolf,
Jacqueline Pauli, Walter Kaufmann (eds.)

Structural behavior of lantern-shaped reticulated shell considering skin effect of perforated aluminum alloy plate

Xiaonong GUO*, Zilin TANG, Liyan JI

*College of Civil Engineering, Tongji University
NO.1239 Siping Road, Shanghai, 20092, China
guo-xiao-nong@tongji.edu.cn

Abstract

With the rapid development of aluminum alloy reticulated shells, the variety of forms for these structures and their enclosing systems has significantly increased. A practical project has innovatively adopted a lantern-shaped double-layer reticulated shell with perforated aluminum alloy plates. Traditionally, enclosure structures are often overlooked as safety reserves without considering their influence on the overall structural performance. This approach leads to inconsistencies in the stress distribution and unnecessary waste of materials. This paper established the shear models for perforated aluminum alloy plates using ANSYS software. The influence of perforation rate on plate deformation was analyzed and the shear stiffness formula was derived through extensive numerical results. Based on the criterion of stiffness equivalence, the perforated aluminum alloy plate was equivalent to a cross-bars model. This simplified model was then applied to the lantern-shaped reticulated shell to study the influence of the skin plates on the performance of the shells. Considering the skin effect of perforated aluminum alloy plates, the ultimate load of the shells can be increased by up to 230%, and the maximum deformation can be reduced by up to 95%.

Keywords: aluminum alloy reticulated shell, perforated aluminum alloy plate, skin effect.

1. Introduction

As research on material properties and structural performance continues to advance, aluminum alloy structures are increasingly utilized in practical projects, featuring diverse shapes and forms of enclosure structures. To meet the requirements of aesthetics, ventilation, lighting, and architectural design, perforated aluminum alloy plates are widely employed in the enclosure structure. An innovative aluminum alloy double-layer reticulated shell structure with perforated aluminum alloy plates is used in a practical project[1], as shown in Figure 1. In structural analysis, enclosure structures typically serve merely as safety reserve, overlooking their influence on the overall performance. However, the enclosure structure and the main structure jointly sustain external loads and undergo deformation. The effect of the enclosure plate, also known as the skin plate, on the overall performance of the structure, including the ultimate load and overall stiffness, is referred to as the skin effect[2].

Since the early 1950s, extensive research has been conducted into the skin effect in building structures. Recognizing that the skin plate primarily transfers force through shear in the overall structure, scholars have proposed some simplified calculation methods and formulas for its shear performance. Notably, Nilson[3] and Bryan[4] conducted shear tests on 50 steel deck plates to explore the influence of parameters such as waveform, wave height, plate thickness, and plate span on the stiffness and strength of skin plates. Based on the test result, they derived formulas for shear stiffness and shear strength of skin plates.

To investigate the influence of skin plates on the overall structural performance, Wrzesien[5] conducted a foot-size experiment of a six-bay cold-formed portal frame, which showed that the horizontal stiffness of the structure with skin plates was increased by about ten. Moreover, Nagy[6] observed that the ultimate load of the portal frame could be increased by up to 50 percent in certain cases. Further research indicates that considering the skin effect can lead to potential savings of up to 10% in the total cost of steel structures[7].

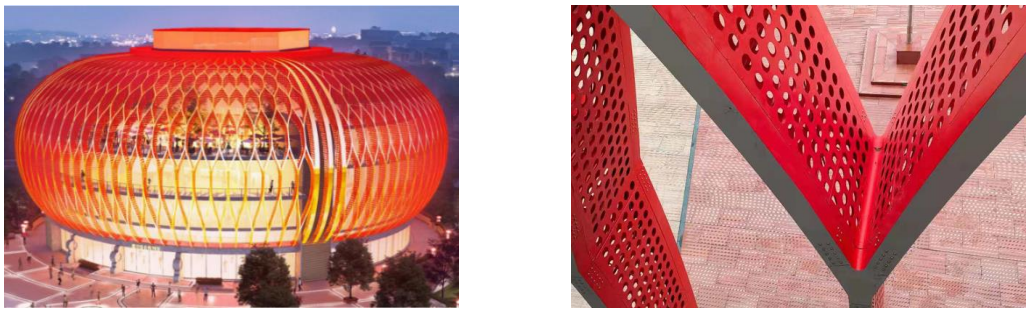

(a) Lantern-shaped reticulated shell structure (b) Perforated aluminum alloy plates

Figure 1: A practical aluminum alloy reticulated shell structure with perforated aluminum alloy plates

Nevertheless, the research on the skin effect is still mainly focused on light steel structures such as portal frames, utilizing steel deck plates for most skin plates. The skin effect of aluminum alloy plates in aluminum alloy spatial structure is less studied, but in fact, its significance in aluminum alloy structures is substantial[8]. Liu[9] found that incorporating skin plates in aluminum alloy reticulated shells can triple the ultimate load compared to shells without skin plates. Similarly, Guo[10] discovered that the ultimate load of aluminum alloy reticulated shells considering the skin effect can be increased by 10-20% when the aluminum alloy skin plates are semi-rigidly connected. Research on perforated aluminum alloy plates in aluminum alloy spatial structures remains limited.

Our team has conducted two series of shear tests on perforated aluminum alloy plates and derived a formula for the shear strength of perforated plates through parametric analysis[11]. This paper primarily examined the influence of perforation rate on the shear stiffness of aluminum alloy plates using finite element analysis and fitted the shear stiffness formula for perforated aluminum alloy plates. According to the stiffness equivalence criterion, a simplified calculation method for the perforated skin plates was proposed, which is conveniently applied to the overall analysis model of the reticulated shells. Finally, the simplified model was applied to the lantern-shaped reticulated shell structure, and the effects of the perforated aluminum alloy plates on the performance of the reticulated shell were investigated.

2. Finite element model of shear perforated aluminum alloy plate

2.1 Shear test of perforated aluminum alloy plates

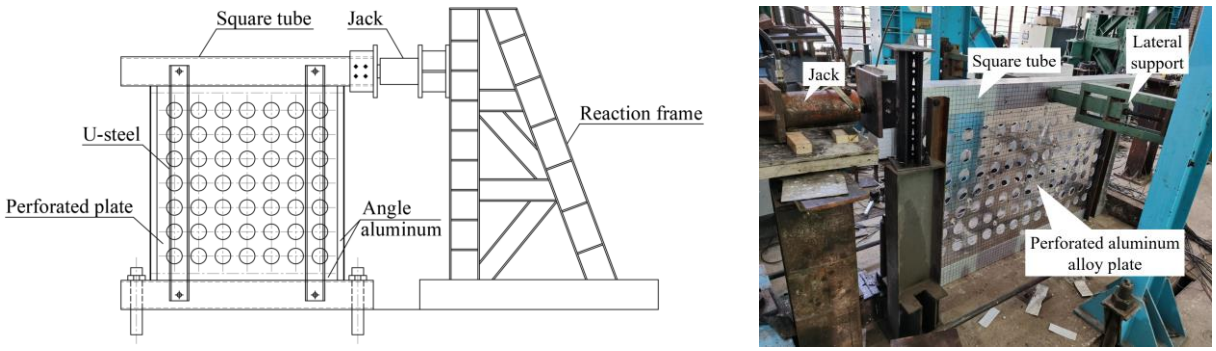

Figure 2: Test setup

To study the shear performance of perforated aluminum alloy skin plates, literature[11] conducted shear tests on two differently sized specimens labeled BJ-A and BJ-B, measuring 1000 mm×1000 mm and 2000 mm×1000 mm, respectively. The plates featured 80mm diameter holes spaced 125 mm center-to-center. The test setup is shown in Figure 2, where a set of opposite sides of the plates are connected with square rods by angles, with one side fixed and horizontal displacement applied to the other side. Upon reaching ultimate loads, both specimens exhibited local buckling. BJ-A developed a single noticeable bulging half-wave, while BJ-B displayed three bulging half-waves (two protruding and one concave), as illustrated in Figure 3. Figure 4 presents the in-plane load-displacement curves for both specimens.

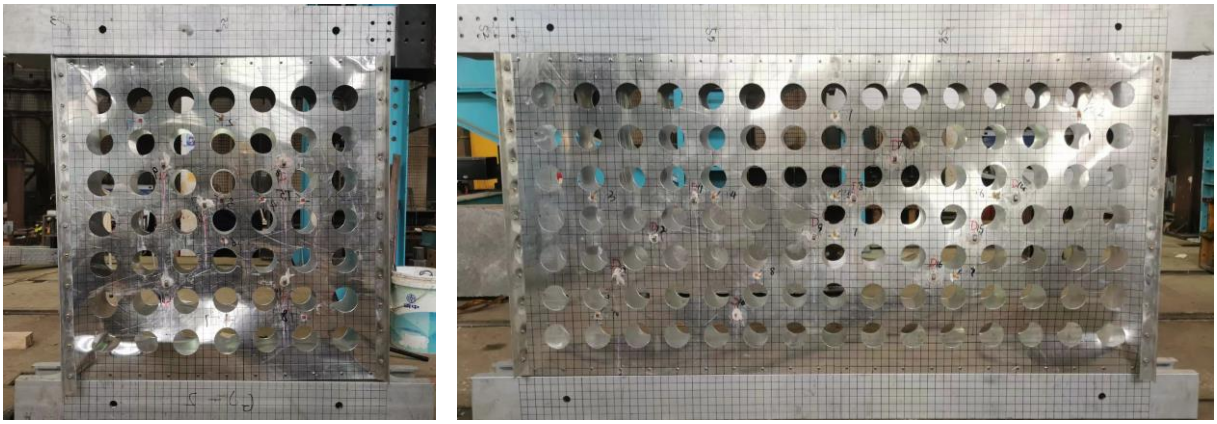

(a) BJ-A (b) BJ-B

Figure 3: Failure mode of specimens

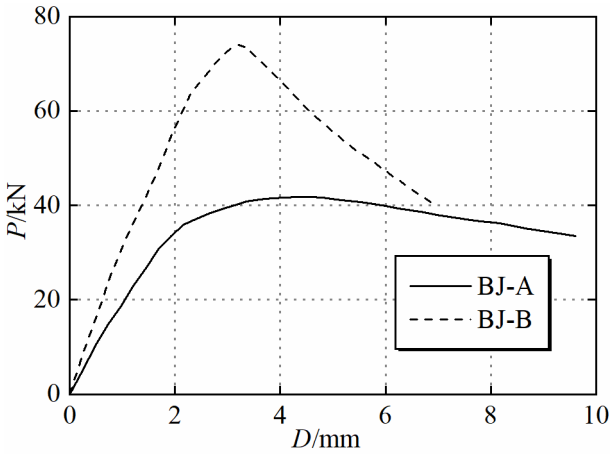

Figure 4: In-plane load-displacement curves of specimens

2.2 Finite element modeling

The ANSYS software was employed to establish a simplified finite element model for the shear tests on the perforated aluminum alloy plates described in Section 2.1, as shown in Figure 5. The plate was simulated by SHELL181 elements. Given that the axial stiffness of the peripheral support rods is much larger than the in-plane shear stiffness of the plate, it is reasonable to assume that the measured displacements reflect only the deformations of the plate, ignoring the deformations of the square tubes. In the finite element model, one side of the plate was fully hinged, while the opposite side was constrained to horizontal movement only, aligning with the direction of shear. The shear load was applied using the SURF153 elements. The U-steels were simulated by BEAM3 elements with ends coupled with the plate. The bilinear material model was selected for the aluminum alloy plate, and its physical and mechanical properties were taken from the data measured in the tests in the literature[11], as presented in Table 1. Figure 6 shows the out-of-plane displacement cloud of the perforated plate under shear in the finite element model. At the limit state, the bulging waves, indicative of damage, emerge.

Table 1: Material properties of aluminum alloy plate in finite element model

Grades	Yield strength $f_{0.2}$/MPa	Tensile strength f_u/MPa	Modulus of elasticity E/MPa	Elongation δ_5/%
3003-H24	103.6	115.6	51487.9	10.27

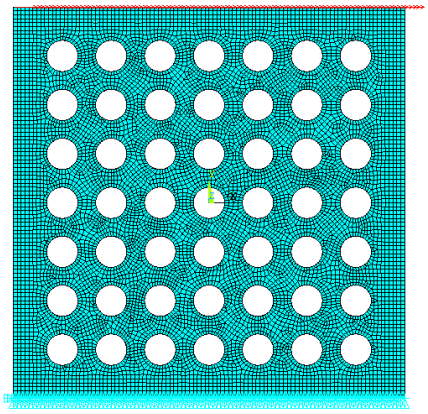

Figure 5: Shear model of perforated aluminum alloy plate

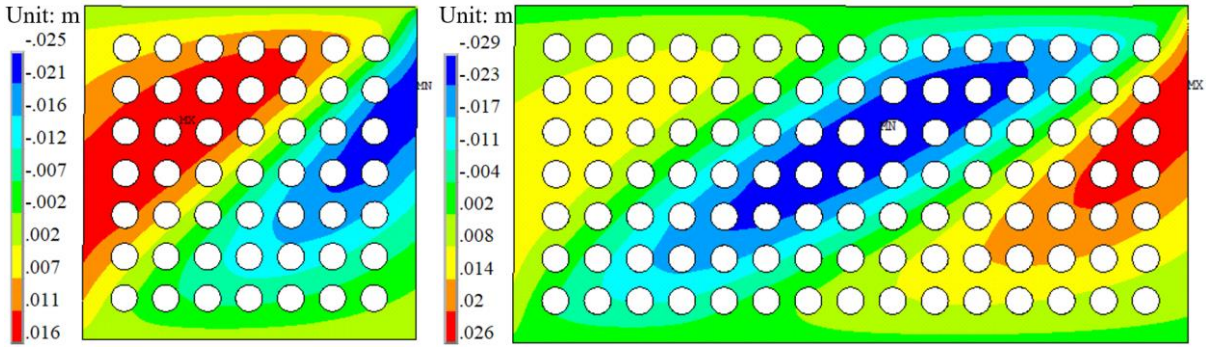

(a) BJ-1 (b) BJ-2

Figure 6: Out-of-plane deformation diagrams of finite element models

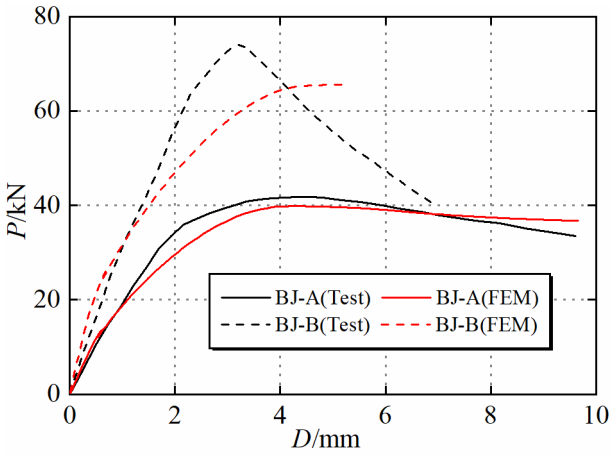

Figure 7: In-plane load-displacement curves of finite element models and tests

Figure 7 compares the in-plane load-displacement curves between finite element models and tests. The *Design of Cold-formed Steel Diaphragms* (AISI)[12] specifies that the shear stiffness of the skin plate

can be determined by the cutline stiffness at the load value of $0.4P_u$, where P_u is the ultimate load of the skin plate. Table 2 lists the comparison of the results from the finite element models and tests, which verifies the accuracy of the finite element model.

Table 2: Comparison of finite element models and tests

Specimen number	Shear stiffness of the specimen k_t/kN·mm^{-1}	Shear stiffness of the finite element model k_f/kN·mm^{-1}	Error in shear stiffness /%	Ultimate load of the specimen P_t/kN	Ultimate load of the finite element model P_f/kN	Error in ultimate load /%
BJ-A	19589	20143	2.8	41.8	39.8	-4.8
BJ-B	31495	36733	16.6	74.0	65.5	-11.5

3. Formula for shear stiffness of perforated aluminum alloy plate

For an unperforated aluminum alloy plate with length *a*, width *b*, and thickness *t*, the theoretical shear stiffness *k*, disregarding initial imperfection, is

$$k = \frac{1}{\frac{4b^3}{Eta^3} + 1.2\frac{2(1+v)b}{Eta}} \tag{1}$$

where *E* and *v* represent the modulus of elasticity and Poisson's ratio of the plate, respectively.

To explore the influence of perforation rate on the shear stiffness of the perforated aluminum alloy plates, a series of finite element models with varying geometric dimensions and perforation rates was developed based on the model presented in Section 2. Only the plate component was established in the parameter analysis model and the boundary conditions were set to be simply supported on all four sides, reflecting the actual construction. Table 3 provides detailed information about these models.

Table 3: Summary of model information

Serial number	Plate length *a*/mm	Plate width *b*/mm	Number of holes *N*	Plate thickness *t*/mm	Hole diameter *d*/mm
A-Φ	1000	1000	49	2,4,6	0,10,20,30,40,50, 60,70,80,90,100,110
B-Φ	1500	1000	77	4	0,10,20,30,40,50, 60,70,80,90,100,110
C-Φ	2000	1000	105	4	0,10,20,30,40,50, 60,70,80,90,100,110

Figure 9 shows the shear stiffness curves of perforated plates with different length-width ratios and width-thickness ratios changing with the perforation rate. Notably, the larger the perforation rate, the lower the shear stiffness of the plate. To quantify this effect, the influence coefficient of perforation, α_φ, is introduced. This coefficient is defined as the ratio of the shear stiffness of the perforated skin plate, k_φ, to that of the unperforated skin plate, $k_{\varphi=0}$, and is calculated as Equation (2):

$$\alpha_\varphi = \frac{k_\varphi}{k_{\varphi=0}} \tag{2}$$

The influence coefficient of perforation for each model was calculated, as depicted in Figure 9. The length-width ratios and width-thickness ratios of the plate have minimal effect on the α_φ. The equation for the influence coefficient of perforation was fitted, as shown in Equation (3):

$$\alpha_\varphi = 1.7\varphi^2 - 2.7\varphi + 1 \tag{3}$$

where $0 \leqslant \varphi < 50\%$.

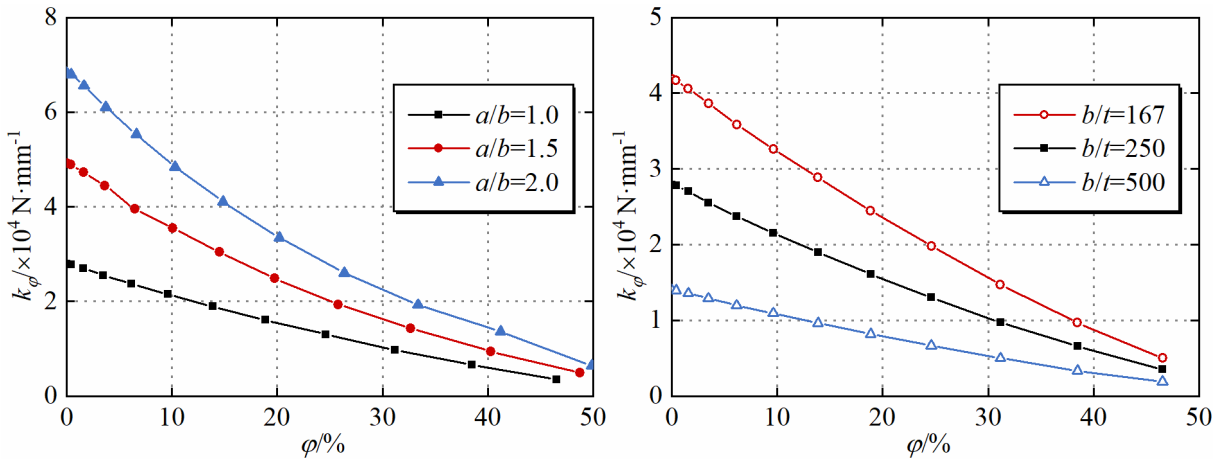

(a) Plates with different length-width ratios (b) Plates with different width-thickness ratios

Figure 8: Effect of perforation rate on the shear stiffness

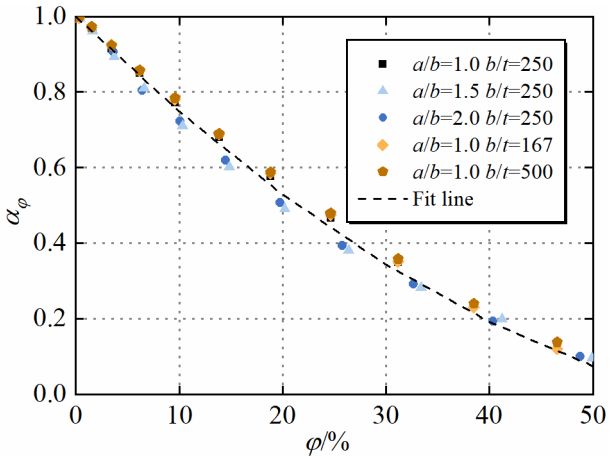

Figure 9: Fit line of the influence coefficient of perforation

Therefore, the empirical formula for the shear stiffness of the perforated plate can be calculated according to Equation (4):

$$k_\varphi = a_\varphi k = \frac{1.7\varphi^2 - 2.7\varphi + 1}{\frac{4b^3}{Eta^3} + 1.2\frac{2(1+v)b}{Eta}} \tag{4}$$

4. Simplified model of perforated plate

4.1 Modelling

Incorporating numerous shell elements into a complex spatial structure model to consider the skin effect can result in computational inefficiency. To enhance computational efficiency while ensuring a certain level of accuracy, this paper proposed a simplified model for simulating perforated aluminum alloy plates with cross-bars. Since the skin plate is primarily subjected to the shear transmitted from the edge members in the structure, this simplified model is equivalent based on the criterion of shear stiffness equivalence.

Figure 10 displays the deformations of a perforated skin plate with length a and width b, as well as its simplified model, under shear load P. The shear deformation δ_A of the skin plate under shear load P is:

$$\delta_{\mathrm{A}} = \frac{P}{k_{\varphi}} \tag{5}$$

In the simplified model, only the elongated bar AD is stressed, and the axial force N_{AD} of the AD bar is:

$$N_{\mathrm{AD}} = \frac{P}{\cos\theta} = \frac{P\sqrt{a^2+b^2}}{a} \tag{6}$$

Then the shear deformation δ_{B} of the simplified model is:

$$\delta_{\mathrm{B}} = l_{\mathrm{DD_1}} = \frac{l_{\mathrm{DD_2}}}{\cos\theta} \approx \frac{N_{\mathrm{AD}} l_{\mathrm{AD_2}}}{EA\cos\theta} = \frac{P\cdot(a^2+b^2)^{3/2}}{EAa^2} \tag{7}$$

where θ——the angle between the bar and the long side of the plate;

A——equivalent cross-sectional area of the bar.

Based on the principle of stiffness equivalence, the shear deformations of the skin plate and the simplified model are the same under the top concentrated force P, expressed as:

$$\delta_{\mathrm{A}} = \delta_{\mathrm{B}} \tag{8}$$

Substituting Equation (5) and Equation (7) into Equation (8), the equivalent cross-sectional area A of the bar is obtained:

$$A = \frac{k_{\varphi}\cdot(a^2+b^2)^{3/2}}{Ea^2} \tag{9}$$

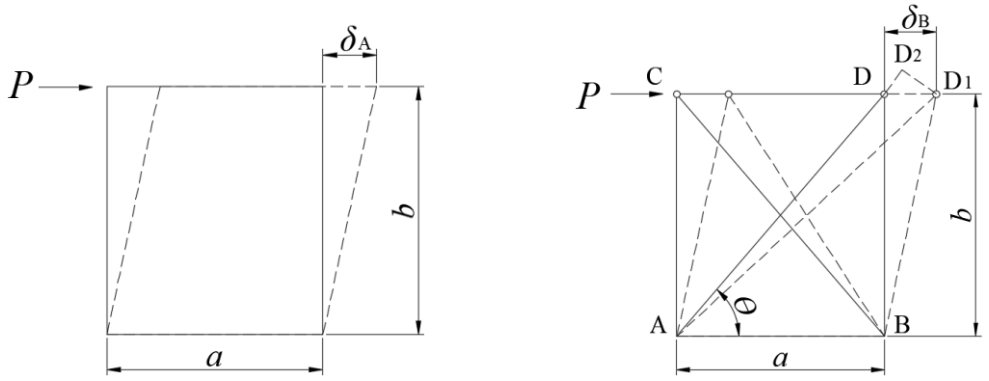

(a) Deformation of the skin plate (b) Deformation of the simplified model

Figure 10: Deformation of two models under shear

4.2 Model validation

To validate the effectiveness of the above simplified model, ANSYS finite element software was used to establish a simplified model of the A-Φ model with a thickness of t=6 mm and a hole diameter of d=60 mm in Section 3, allowing for a comparison of the two models under shear. In the simplified model, the cross-bars employed LINK180 elements, configured as tension-only elements, while BEAM3 elements were used for the edge members. The boundary conditions remained consistent with those of the models in Section 3. According to Equation (4), the shear stiffness k_{φ} of the perforated plate is 28574 N/mm. The equivalent cross-sectional area of the simplified model is obtained from Equation (9):

$$A = \frac{k_{\varphi}\cdot(a^2+b^2)^{3/2}}{Ea^2} = \frac{28574\times(1000^2+1000^2)^{3/2}}{51487.9\times1000^2} = 1569.7\mathrm{mm}^2 \tag{10}$$

Figure 11 shows the deformations of both models under the same shear loads, showing nearly identical shear deformations at the apex side. Figure 12 presents the load-displacement curves of both models.

The results reveal that the calculation results of the original and simplified model are close, indicating a high level of accuracy in the simplified model.

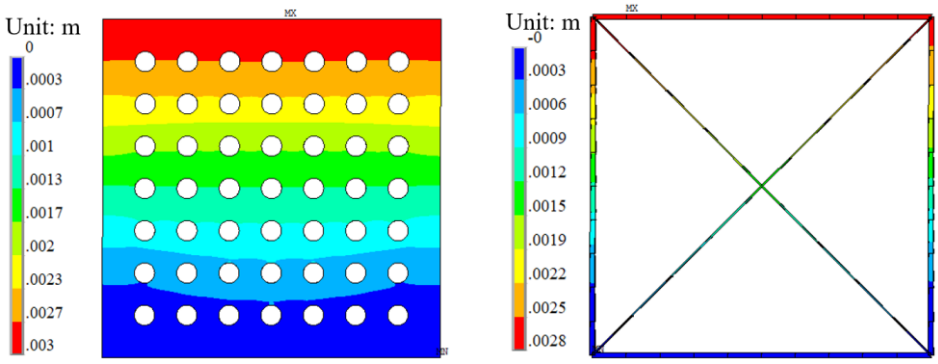

(a) Original model (b) Simplified model

Figure 11: Deformations of original and simplified models

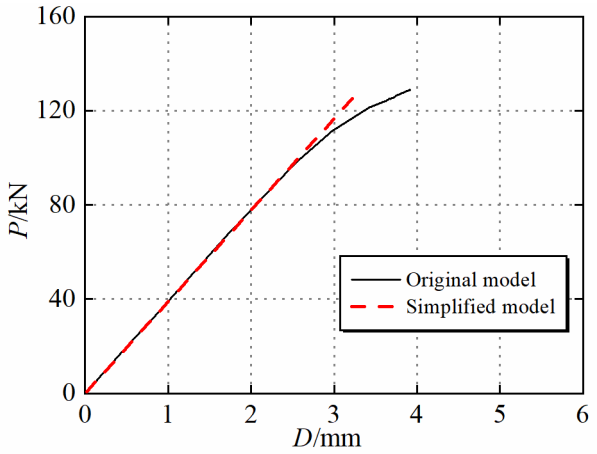

Figure 12: Load-displacement curves for original and simplified models

5. Overall performance of reticulated shell with perforated skin plate

A practical aluminum alloy reticulated shell structure with perforated skin plates[1] was taken as an example to analyze the effect of perforated skin plates on the overall performance of the structure. The structure is a double-layer lantern-shaped reticulated shell, primarily composed of aluminum alloy, standing approximately 25 m in height with a maximum diameter of about 68 m. It is characterized by a centrosymmetric arrangement and reinforced by four bays of vertical Q355 steel trusses to ensure structural stiffness. The aluminum alloy reticulated shell is made of 6082-T6 □150×8 mm square tubes, and the double layer shells are connected by [60×30 mm channels. The enclosing structure employs perforated 3003-H24 aluminum alloy plates.

Three full-span homogeneous load combinations are considered for stability analysis in this paper, detailed in Table 4. The constant load and live load were set as 0.5 kN/m^2, while the basic wind pressure was 0.3 kN/m^2.

Table 4: Load combinations in structural stability analysis

Combination number	Combinatorial principle	Instructions
1	1.0*G+1.0*Q	Constant load + live load
2	1.0*G+1.0*Q+0.6*W1	Constant load + live load + wind load(0 degrees)
3	1.0*G+1.0*Q+0.6*W2	Constant load + live load + wind load(45 degrees)

ANSYS finite element software was used to establish the models with and without skin plate respectively, as shown in Figure 13. The main structural members were simulated by BEAM188 elements, while the skin plates were simulated by the simplified model proposed in Section 4. Due to the structural complexity, the dimensions of each perforated plate are not the same. For computational convenience, all skin plates were uniformly assumed to be of intermediate size, measuring 2019mm in length, 942 mm in width, and 4 mm in thickness, with a perforation rate of 24.6%. According to Equation (4) and (9), the equivalent cross-sectional area of the cross-bar is 2556.7 mm^2.

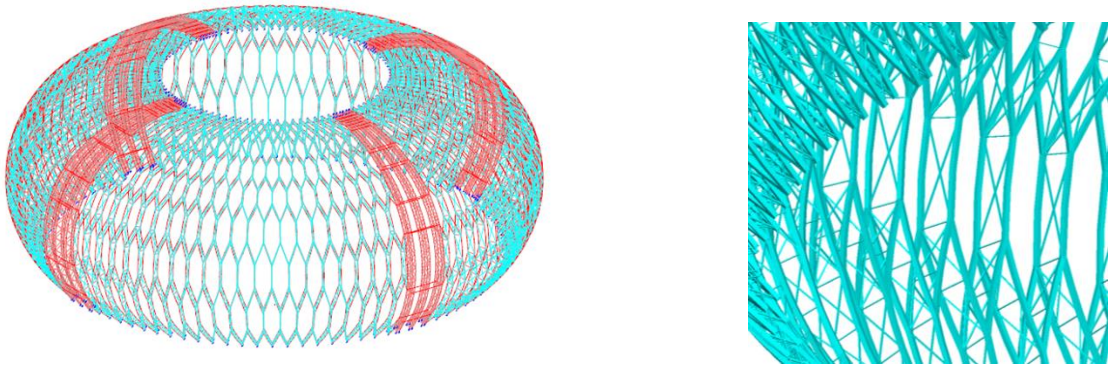

(a) Main structure (b) Simplified models of skin plates in the overall structure

Figure 13: Model of a practical double-layer reticulated shell structure

5.1 Static performance of the structure

The maximum deformations and the maximum axial forces of the two models under static analysis are listed in Table 4. The skin effect can enhance the stiffness of the structure to a certain extent and reduce the internal forces of the members. Specifically, maximum deformations decreased by 95% and the maximum axial forces decreased by 73% under load combination 1.

Table 5: Comparison of structural static performance

Combination number	Maximum deformation of non-skin model /m	Maximum axial force of non-skin model /kN	Maximum deformation of skin model /m	Maximum axial force of skin model /kN	Skin effect on displacement	Skin effect on axial force
1	0.1065	204.54	0.0052	56.17	-95%	-73%
2	0.1195	276.79	0.0528	196.81	-56%	-29%
3	0.1205	260.64	0.0616	179.53	-49%	-31%

5.2 Non-linear stability of the structure

According to the *Technical Regulations for Spatial Mesh Structures* (JGJ7-2010)[13], initial geometric imperfection was introduced by consistent imperfection modal method, with the defect magnitude set as $L/300$, where L represents the span of the shell. Table 6 presents the non-linear ultimate loads of two kinds of reticulated shells under three load combinations. The ultimate load of the shell can be increased by up to 230% under load combination 3.

Table 6: Comparison of structural non-linear stability

Combination number	Overall stability factor of non-skin model	Overall stability factor of skin model	Skin effect on Overall stability
1	11.50	36.67	219%
2	10.87	33.53	208%
3	10.64	35.15	230%

6. Conclusion

This paper studied the shear stiffness of perforated aluminum alloy plates and their effect as enclosure structures on the overall performance of aluminum alloy spatial structure. The main conclusions are summarized as follows:

(1) Perforation reduces the shear stiffness of the aluminum alloy plate. The finite element model for shear resistance of perforated aluminum alloy plates was established and validated through comparison with experimental results. An empirical equation for the shear stiffness of the plate was fitted based on the finite element models;

(2) To improve the computational efficiency of the overall structure considering the skin effect, a simplified model with cross-bars equivalent to perforated aluminum alloy plates was proposed and its reliability was verified;

(3) Taking a practical double-layer aluminum alloy reticulated shell structure as an example for structural analysis considering the skin effect, it was found that the maximum displacement of the structure can be reduced by 95% and the ultimate load can be increased by 230% after accounting for skin plates.

References

[1] Y. D. Zhou, C. H. Wang, H. Ouyang, J. Liu and X. N. Guo, "An Introduction to the Design of a Lantern-Shaped Aluminum Alloy Space Structure," *Nonferrous Metal Processing*, vol. 50, no. 4, pp. 55-60, 2021. (in Chinese)

[2] R. T. Malone and R. W. Rice, "The Analysis of Irregular Shaped Structures: Diaphragms and Shear Walls," *Mcgraw Hill*, New York, 2012.

[3] A. H. Nilson, "Shear Diaphragms of Light Gauge Steel," *Journal of the Structural Division*, vol. 86, no. 3, pp. 111-139, 1960.

[4] E. R. Bryan and W. M. El-Dakhakhni, "Shear Flexibility and Strength of Corrugated Decks," *Journal of the Structural Division*, vol. 94, no. 11, pp. 2549-2580, 1968.

[5] A. M. Wrzesien, B. P. Lim James and Y. X. Xu, "Effect of Stressed Skin Action on the Behaviour of Cold-Formed Steel Portal Frames," *Engineering Structures*, vol. 105, pp. 123-136, 2015.

[6] Z. Nagy, A. Pop, and I. Mois, "Stressed Skin Effect on the Elastic Buckling of Pitched Roof Portal Frames," *Structure*, vol. 8, pp. 227-244, 2016.

[7] E. R. Bryan, "The Stressed Skin Design of Steel Buildings," *Crosby Lockwood Staples*, London, 1973.

[8] Y. Z. Wu, "Study on Skin Effect of Single-Layer Aluminum Reticulated Shells," *Building Structure*, vol. 48, no. S2, pp. 1018-1021, 2018. (in Chinese)

[9] H. B. Liu, Z. H. Chen and S. Xu, " Structural Behavior of Aluminum Reticulated Shell Structures Considering Semi-Rigid and Skin Effect," *Structural Engineering and Mechanics*, vol. 54, no. 1, pp. 121-133, 2015.

[10] X. N. Guo, Z. L. Tang, X. Y. Chen, "Non-Linear Stability of Aluminum Alloy Single-Layer Reticulated Shells Considering Stressed-Skin Effect," *International Journal of Structural Stability and Dynamics*, pp. 2550013, 2025.

[11] X. N. Guo, L. Y. Ji, J. Liu, J. H. Luo, H. Ouyang, "Research on Shear Performance of Perforated Aluminium Alloy Plates," *Journal of Building Structures*, vol. 44, no. 8, pp. 185-195, 2023. (in Chinese)

[12] "Design of Cold-Formed Steel Diaphragms," AISI.

[13] JGJ 7-2010, "Technical Specification for Space Frame Structures," Beijing, 2010. (in Chinese).